

A Numerical Investigation of Stagnation Flow

J. G. BAIN and C. A. J. FLETCHER

University of Sydney, Australia.

ABSTRACT

An efficient computational algorithm is used to model the two-dimensional flow field upstream of a surface mounted bluff body. Computationally, the Bernoulli variable, H , is introduced in place of the pressure. This variable has the advantage of changing less than the pressure in certain critical parts of the flow domain. The incompressible Navier-Stokes equations, written in terms of u , v and H , are solved using the efficient group split finite element formulation (Fletcher; 1984, 1985). Numerical solutions have been computed for a flow field which includes a separation bubble having both laminar separation and laminar attachment.

INTRODUCTION

The flow in the stagnation region of a bluff body intersecting a flat plate is complicated by the accumulation of lateral vorticity ahead of the body and the redeployment of this vorticity into the streamwise direction as the flow sweeps past the body. The net effect is a separation of the symmetry line flow ahead of the body and the appearance of a horseshoe vortex structure wrapped around the body; both Thwaites (1960) and Hunt et al. (1978) illustrate this phenomenon.

Flows of this type occur at wing/body junctions of aircraft, endwall/turbine interfaces in turbomachinery and around bridge piers in rivers. Practical interest exists in predicting such flows to alleviate, ultimately, the reduction in lift and increase in drag for the first case, the loss of turbine/compressor efficiency in the second case and the scouring of river beds in the third case.

This three-dimensional flow behaviour has been examined experimentally by Stanbrook (1959), Peake et al. (1965), Shabaka (1979) and Langston (1980), amongst others. Computational models for this type of flow have, typically, been based on boundary layer analysis which is capable of predicting the upstream separation but not the complex vortical interactions, (Sharma and Graziani, 1983). The obvious need for an efficient computational model which will accurately predict the flow behaviour near a wing/body junction is the motivation behind the present work.

The problem investigated here is that of a two-dimensional decelerating flow upstream of a surface mounted bluff body. This flow is not totally unlike a cross-section - through the plane of symmetry - of the three-dimensional junction problem, although in two dimensions the flow is unable to "escape" around the side of the body. In the present computational problem the incompressible Navier-Stokes equations will be solved. A conventional pseudo-transient formulation in terms of the primitive variables, u, v, p (in two-dimensions) is rather uneconomical. For incompressible flow the uncoupling of the continuity equation is an added complication. In this paper a different strategy is adopted. The Bernoulli variable, H , is used instead of the pressure, since this variable will change less than the pressure in certain critical parts of the region. The Navier-Stokes equations can now be written in terms of u, v and H (see equations (2), (3) and (4) below). The

numerical solution of these equations is structured as follows. First the x -momentum equation is put into an equivalent unsteady form and then discretised into uncoupled systems of algebraic equations for each grid-line, (Fletcher, 1984; Fletcher and Srinivas, 1983, 1985). Each step in time will therefore result in a correction to the u velocity component. The y -momentum equation and the continuity equation will provide an appropriate update of H and v at each time step. A pseudo-transient correction to the v velocity component is obtained in a similar fashion, in this case the roles of u and v will be reversed. This sequential algorithm will be explained more fully in a later section. The numerical solutions show, for Reynolds numbers of 50 and 100, the presence of a separation bubble having both laminar separation and laminar attachment.

EQUATIONS AND BOUNDARY CONDITIONS

For external flows that are inviscid and irrotational far from an isolated body it is advantageous, computationally to introduce the Bernoulli function in place of the pressure. In two dimensions the Bernoulli function can be written - in dimensional variables - as

$$H = p + \rho(u^2 + v^2)/2 \quad (1)$$

In the inviscid and irrotational region away from the body H becomes constant whereas the pressure, p , adjusts to the changing velocity field. This follows directly from the governing equations for steady two-dimensional incompressible viscous flow, written in non-dimensional form as,

$$vu_y - vv_x + H_x - \nabla^2 u / Re = 0 \quad (2)$$

$$-uu_y + uv_x + H_y - \nabla^2 v / Re = 0 \quad (3)$$

$$u_x + v_y = 0 \quad (4)$$

where the Reynolds number is given by $Re = U_\infty L / \nu$, (L a suitable lengthscale). Equations (2) and (3) are the x and y momentum equations respectively and equation (4) is the continuity constraint. In the inviscid outer region the governing equations will reduce to Laplace's equation, $\nabla^2 \phi = 0$, where ϕ is the velocity potential.

Appropriate boundary conditions for the above equations can be derived for a particular domain of interest. For the "corner" geometry (which is infinite in both coordinate directions - see Figure 1) the inflow and outflow conditions play an important role in determining the nature of the solution. Here the extent of the computational domain is assumed large enough so that boundary-layer approximations can be applied at both inflow and outflow boundaries. At the inflow boundary a Dirichlet condition is given for v ; u is determined from the interior solution together with the boundary layer assumption that $u_{yy} = 0$ at inflow. H is determined by integrating a reduced form of the x -momentum equation along the inflow boundary. H is given a constant value at the grid point furthest from the corner, here the flow is assumed inviscid and irrotational. At the solid boundaries $u=v=0$ and H is calculated from the interior solution. At the outflow

boundary $u_{xx} = 0$ and a reduced form of the y-momentum equation is used to calculate H.

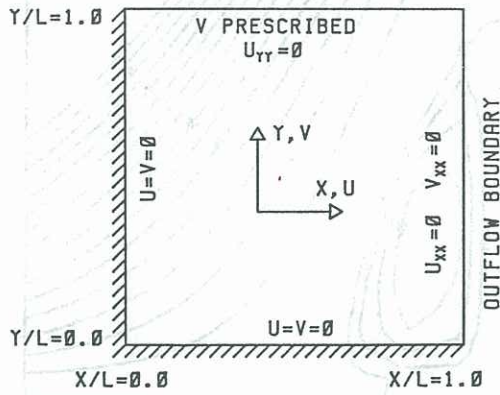


Fig. 1: Computational domain and boundary conditions.

NUMERICAL FORMULATION

For the present problem an efficient sequential algorithm can be constructed as follows. First eq. (2) is written - with the aid of the continuity equation - in pseudo-transient conservation form,

$$u_t + (H + u^2/2 - v^2/2)_x + (uv)_y - \nabla^2 u / \text{Re} = 0 \quad (5)$$

where time will be used to provide a convenient iteration path.

A group finite element formulation (Fletcher, 1983) with linear Lagrange rectangular elements is introduced. This produces the following semi-discrete form of eq. (5) (for internal nodes),

$$M_x \otimes M_y u_t = -M_y \otimes L_x (H + u^2/2 - v^2/2) - M_x \otimes L_y (uv) + [M_y \otimes L_{xx} + M_x \otimes L_{yy}] u / \text{Re} = \text{RHS} \quad (6)$$

where \otimes denotes the tensor product and the directional mass operators (Fletcher and Srinivas, 1984, 1985) are defined by

$$M_x = \{1/6, (1+r_x)/3, r_x/6\}, M_y^t = \{r_y/6, (1+r_y)/3, 1/6\} \quad (7)$$

and directional difference operators by

$$L_x \equiv \frac{1}{2}[-1, 0, 1]/\Delta x \text{ and } L_{xx} \equiv \{1, -(1+1/r_x), 1/r_x\}/\Delta x^2 \quad (8)$$

similarly for L_y and L_{yy} . In eqs. (7) and (8) r_x and r_y are the grid growth ratios, i.e.

$$r_x = (x_{i+1} - x_i)/(x_i - x_{i-1}), r_y = (y_{j+1} - y_j)/(y_j - y_{j-1}) \quad (9)$$

Since only the steady-state solution of eq. (6) is of interest a linearised backward Euler (Newton-like) time discretisation is introduced as

$$M_x \otimes M_y \Delta u^{n+1} = \Delta t \text{RHS}^{n+1} = \Delta t \text{RHS}^n + (\partial \text{RHS} / \partial u) \Delta u^{n+1} \quad (10)$$

where $\Delta u^{n+1} = u^{n+1} - u^n$.

Equation (10) represents a linear system of equations for the corrections Δu^{n+1} , and can be solved approximately by introducing a very efficient coordinate splitting or factorisation (Fletcher and Srinivas 1984, 1985). This leads to the following two stage algorithm

$$[M_x - \Delta t \{(1/\text{Re})L_{xx} - 2L_x u\}] \Delta u^* = \Delta t \text{RHS}^n \quad (11a)$$

$$[M_y - \Delta t \{(1/\text{Re})L_{yy} - L_y v\}] \Delta u^{n+1} = \Delta u^* \quad (11b)$$

At each stage the solution of (11a) or (11b) involves only operators associated with a particular coordinate direction. This permits a decoupling of the equations and the efficient implementation of banded Gauss elimination along each grid-line in turn. The RHS term has been treated as a function of u only. Strictly it is also a function of v and H . However to avoid the solution of relatively expensive block tridiagonal systems the remaining momentum equation, (3), is exploited (at different stages of the sequential algorithm) to obtain updates of H and v for each step of the iterative solution of equation (11).

Along the inflow boundary H is determined from a reduced form of the x-momentum equation - the u_{yy} term is assumed negligible here. With H a known constant in the far field, this equation is integrated towards the side wall. Utilizing equation (4), the y-momentum equation can be written in the form,

$$(H - u^2/2 + u_x/\text{Re})_y = v_{xx}/\text{Re} - uv_x \quad (12)$$

Integrating (12) from the inflow boundary (where H is now known) toward the solid boundary will determine H over the remainder of the domain. With this update of H in the RHS of equation (6), a subsequent iteration of equation (11) will produce a new correction for the u velocity component. Having updated u , the v component can be calculated from the continuity equation. A one-dimensional finite element discretization of (4) produces

$$L_y v = -M_y q \quad (13)$$

where $q (=u_x)$ is calculated using central differencing. Equation (13) - which is effectively a numerical integration of (4) by Simpson's rule - is marched away from the solid wall up to, but not including, the inflow boundary; v is already prescribed at this boundary. For the first step out from the wall v is calculated using a trapezoidal integration of (4).

In a similar manner a pseudo-transient update of v is carried out by simply reversing the roles of the momentum equations in (5) and (12) and equation (4) now updates u instead of v . These two calculations will follow each other sequentially. Thus, at each pseudo-transient correction of v , say, the RHS term will consist of a recently updated H variable and two velocity components; of which the u component is determined from the previous pseudo-transient step and the v component from the resulting continuity correction.

At the start of the iteration the u and v components are chosen so that the continuity condition will be satisfied throughout the computational domain.

RESULTS AND DISCUSSION

The numerical method described in the preceeding section is illustrated by application to a two-dimensional bluff body flow for the computational domain shown in Figure 1.

Representative streamline patterns produced by the present method are shown in Figures 2, 3 and 4. These results correspond to Reynolds numbers of 10, 50 and 100 respectively. The effect of increasing the Reynolds number can be appreciated by comparing these solutions. In Figure 2, corresponding to the case $\text{Re} = 10$, the fluid is carried around the corner without exhibiting separation. For Reynolds numbers of 50 and 100 (Figures 3 and 4) the deceleration of fluid - due to the upstream bluff boundary - is too severe for a thin boundary layer to be possible at the wall; more and more vorticity accumulates in the ever thickening boundary layer and ultimately separation occurs. In this case, as far as the outer potential flow is concerned, the presence of a separation bubble will effectively change the shape of the rigid boundary. As is evident from Figures 3 and 4 the separation point shifts upstream as the Reynolds number is increased. This behaviour has been noted previously for separated flow, (Leal, 1973; Hancock and Lewis, 1985).

The present results were obtained on a uniform 21×21 grid using a time step of $\Delta t = 0.001$. The "jagged" appearance of the recirculating eddy could be reduced through the introduction of a much finer grid in the neighborhood of the eddy. The precise location of this reduced grid would be determined from the present uniform grid results.

Khosla and Rubin (1983) have developed a finite difference algorithm that shares some common features with the present method. In particular a Bernoulli function is used in place of the pressure and determined from the normal momentum equation. However an auxiliary velocity potential is introduced to satisfy the continuity equation. This same velocity potential provides the complete solution in the outer inviscid region. In the viscous region the u solution comes partly from $\partial\phi/\partial x$ and partly from a viscous component, u_v . Consequently continuity and x -momentum must be solved as a coupled system for ϕ and u_v .

The flow behaviour illustrated here shows similar characteristics to the decelerated flow investigated by Leal (1973), where in that case deceleration is due to an opposing flow rather than a bluff body.

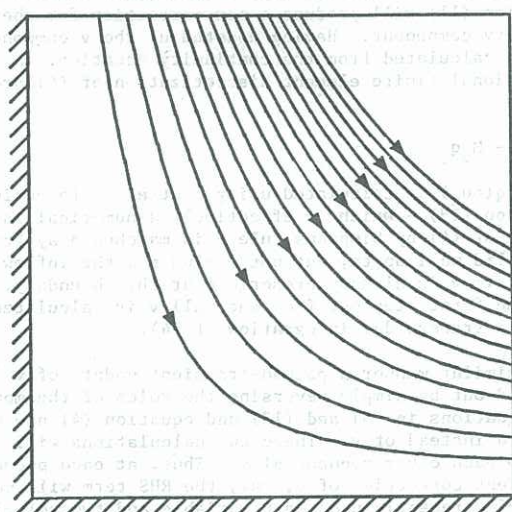


Fig. 2: Streamline pattern, $Re = 10$

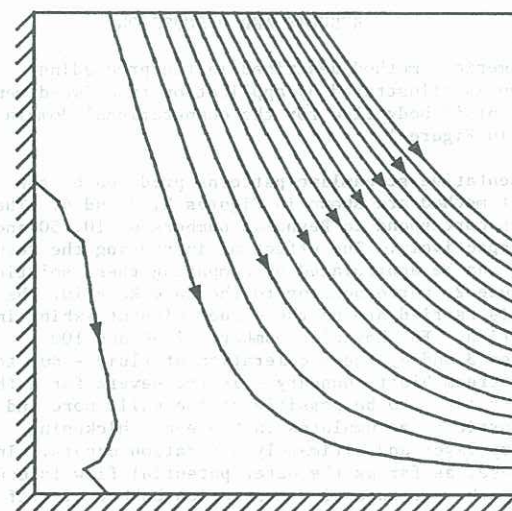


Fig. 3: Streamline pattern, $Re = 50$

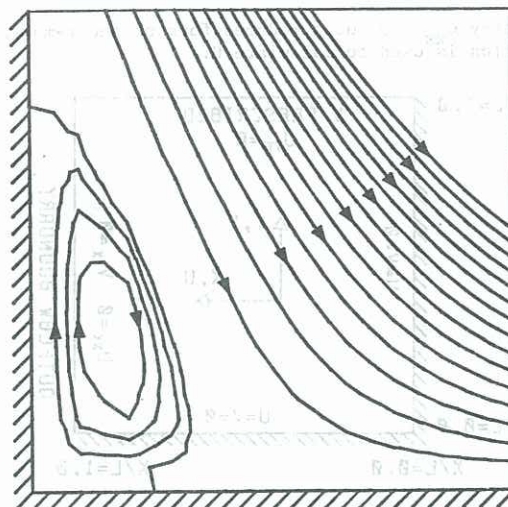


Fig. 4: Streamline pattern, $Re = 100$

CONCLUSION

The two dimensional flow upstream of a surface mounted bluff body has been considered. The incompressible Navier-Stokes equations (written in the primitive variables u , v and H , where H is the Bernoulli variable) were solved using the efficient group split finite element formulation. The numerical results demonstrate the ability of the present algorithm to accurately predict the flow field, which in some cases will include recirculation, over the computational domain. This algorithm is currently being extended to the three-dimensional flow problem upstream of a wing/body junction.

ACKNOWLEDGEMENT

The authors are grateful to the Australian Research Grants Committee for their continuing support.

REFERENCES

- Fletcher, C.A.J. (1983): The group finite element formulation. *Comp. Meth. Appl. Mech. Eng.*, **37** 225-243.
- Fletcher, C.A.J.; Srinivas, K. (1983): Stream function vorticity revisited. *Comp. Meth. Appl. Mech. Eng.*, **41** 297-322.
- Fletcher, C.A.J. (1984): *Computational Galerkin Methods*. Springer-Verlag, New York.
- Fletcher, C.A.J.; Srinivas, K. (1985): Finite Elements in Fluids. (Eds. R.H. Gallagher et al.), **6**, 115-133.
- Hancock, C.; Lewis, E. (1985): The effects of inertia on the structure of viscous corner eddies. *Comp. Fluids*, **13** 47-59.
- Hunt, J.C.R.; Abell, C.J.; Peterka, J.A.; Woo, H. (1978): Kinematical studies of the flows around free or surface-mounted obstacles; applying topology to flow visualization. *J. Fluid Mech.* **86** 179-200.
- Khosla, P.K.; Rubin, S.G. (1983): A composite velocity procedure for the compressible Navier-Stokes equations. *A.I.A.A. J.* **21**, 1546-1551.
- Langston, L.S. (1980): Crossflows in a turbine cascade passage. *J. Engineering for Power*, **102**, 866-874.
- Leal, L.G. (1973): Steady separated flow in a linearly decelerated free stream. *J. Fluid Mech.* **59** 513-535.

- Peake, D.J.; Galway, R.D.; Rainbird, W.J. (1965): The three-dimensional separation of a plane, incompressible laminar boundary layer produced by a Rankine oval mounted normal to a flat plate. NRC of Canada, Aero Rpt. LR-466.
- Schlichting, H. (1968): Boundary Layer Theory. 6th Edn. McGraw-Hill, New York.
- Shabaka, I.M.M.A. (1979): Turbulent flow in an idealised wing-body junction. Ph.D. Thesis, London University.

Sharma, O.P.; Graziani, R.A. (1983): Influence of endwall flow on aerofoil suction surface mid-height boundary layer development in a turbine cascade. J. Engineering for Power, 105 147-155.

Stanbrook, A. (1959): Experimental observation of vortices in wing-body junctions. ARC, R. and M. No. 3114.

Thwaites, B. (ed.): Incompressible Aerodynamics. OUP (1960) p 554.



Figure 1. The block and cylinder.

Figure 2 shows the velocity field in the $x-y$ plane. The velocity components are given by the following equations:

$$u = U_0 \left(1 - \frac{y^2}{b^2} \right) \quad (1)$$

where U_0 is the free-stream velocity, b is the half-width of the channel, and y is the vertical coordinate. The velocity field is shown in Figure 2.

The velocity field is shown in Figure 2. The velocity components are given by the following equations:

$$u = U_0 \left(1 - \frac{y^2}{b^2} \right) \quad (2)$$

$$v = -\frac{U_0}{b^2} y^2 \quad (3)$$

$$w = 0 \quad (4)$$

$$p = p_0 - \frac{1}{2} \rho U_0^2 \left(1 - \frac{y^2}{b^2} \right)^2 \quad (5)$$

$$\rho = \rho_0 \left(1 - \frac{y^2}{b^2} \right) \quad (6)$$

$$\mu = \mu_0 \left(1 - \frac{y^2}{b^2} \right) \quad (7)$$

$$\kappa = \kappa_0 \left(1 - \frac{y^2}{b^2} \right) \quad (8)$$

$$\alpha = \alpha_0 \left(1 - \frac{y^2}{b^2} \right) \quad (9)$$

$$\beta = \beta_0 \left(1 - \frac{y^2}{b^2} \right) \quad (10)$$

$$\gamma = \gamma_0 \left(1 - \frac{y^2}{b^2} \right) \quad (11)$$

$$\delta = \delta_0 \left(1 - \frac{y^2}{b^2} \right) \quad (12)$$

$$\epsilon = \epsilon_0 \left(1 - \frac{y^2}{b^2} \right) \quad (13)$$

$$\zeta = \zeta_0 \left(1 - \frac{y^2}{b^2} \right) \quad (14)$$

$$\eta = \eta_0 \left(1 - \frac{y^2}{b^2} \right) \quad (15)$$

$$\theta = \theta_0 \left(1 - \frac{y^2}{b^2} \right) \quad (16)$$

$$\phi = \phi_0 \left(1 - \frac{y^2}{b^2} \right) \quad (17)$$

$$\chi = \chi_0 \left(1 - \frac{y^2}{b^2} \right) \quad (18)$$

$$\psi = \psi_0 \left(1 - \frac{y^2}{b^2} \right) \quad (19)$$

$$\omega = \omega_0 \left(1 - \frac{y^2}{b^2} \right) \quad (20)$$

$$\sigma = \sigma_0 \left(1 - \frac{y^2}{b^2} \right) \quad (21)$$

$$\tau = \tau_0 \left(1 - \frac{y^2}{b^2} \right) \quad (22)$$

$$\nu = \nu_0 \left(1 - \frac{y^2}{b^2} \right) \quad (23)$$

$$\xi = \xi_0 \left(1 - \frac{y^2}{b^2} \right) \quad (24)$$

$$\eta = \eta_0 \left(1 - \frac{y^2}{b^2} \right) \quad (25)$$

$$\theta = \theta_0 \left(1 - \frac{y^2}{b^2} \right) \quad (26)$$

$$\phi = \phi_0 \left(1 - \frac{y^2}{b^2} \right) \quad (27)$$

$$\chi = \chi_0 \left(1 - \frac{y^2}{b^2} \right) \quad (28)$$

$$\psi = \psi_0 \left(1 - \frac{y^2}{b^2} \right) \quad (29)$$

$$\omega = \omega_0 \left(1 - \frac{y^2}{b^2} \right) \quad (30)$$

$$\sigma = \sigma_0 \left(1 - \frac{y^2}{b^2} \right) \quad (31)$$

$$\tau = \tau_0 \left(1 - \frac{y^2}{b^2} \right) \quad (32)$$

$$\nu = \nu_0 \left(1 - \frac{y^2}{b^2} \right) \quad (33)$$

$$\xi = \xi_0 \left(1 - \frac{y^2}{b^2} \right) \quad (34)$$

$$\eta = \eta_0 \left(1 - \frac{y^2}{b^2} \right) \quad (35)$$

$$\theta = \theta_0 \left(1 - \frac{y^2}{b^2} \right) \quad (36)$$

$$\phi = \phi_0 \left(1 - \frac{y^2}{b^2} \right) \quad (37)$$

The velocity field is shown in Figure 2. The velocity components are given by the following equations:

$$u = U_0 \left(1 - \frac{y^2}{b^2} \right) \quad (38)$$

$$v = -\frac{U_0}{b^2} y^2 \quad (39)$$

$$w = 0 \quad (40)$$

$$p = p_0 - \frac{1}{2} \rho U_0^2 \left(1 - \frac{y^2}{b^2} \right)^2 \quad (41)$$

$$\rho = \rho_0 \left(1 - \frac{y^2}{b^2} \right) \quad (42)$$

$$\mu = \mu_0 \left(1 - \frac{y^2}{b^2} \right) \quad (43)$$

$$\kappa = \kappa_0 \left(1 - \frac{y^2}{b^2} \right) \quad (44)$$

$$\alpha = \alpha_0 \left(1 - \frac{y^2}{b^2} \right) \quad (45)$$

$$\beta = \beta_0 \left(1 - \frac{y^2}{b^2} \right) \quad (46)$$

$$\gamma = \gamma_0 \left(1 - \frac{y^2}{b^2} \right) \quad (47)$$

$$\delta = \delta_0 \left(1 - \frac{y^2}{b^2} \right) \quad (48)$$

$$\epsilon = \epsilon_0 \left(1 - \frac{y^2}{b^2} \right) \quad (49)$$

$$\zeta = \zeta_0 \left(1 - \frac{y^2}{b^2} \right) \quad (50)$$

$$\eta = \eta_0 \left(1 - \frac{y^2}{b^2} \right) \quad (51)$$

$$\theta = \theta_0 \left(1 - \frac{y^2}{b^2} \right) \quad (52)$$

$$\phi = \phi_0 \left(1 - \frac{y^2}{b^2} \right) \quad (53)$$

$$\chi = \chi_0 \left(1 - \frac{y^2}{b^2} \right) \quad (54)$$

$$\psi = \psi_0 \left(1 - \frac{y^2}{b^2} \right) \quad (55)$$

$$\omega = \omega_0 \left(1 - \frac{y^2}{b^2} \right) \quad (56)$$

$$\sigma = \sigma_0 \left(1 - \frac{y^2}{b^2} \right) \quad (57)$$

$$\tau = \tau_0 \left(1 - \frac{y^2}{b^2} \right) \quad (58)$$

$$\nu = \nu_0 \left(1 - \frac{y^2}{b^2} \right) \quad (59)$$

$$\xi = \xi_0 \left(1 - \frac{y^2}{b^2} \right) \quad (60)$$

$$\eta = \eta_0 \left(1 - \frac{y^2}{b^2} \right) \quad (61)$$

$$\theta = \theta_0 \left(1 - \frac{y^2}{b^2} \right) \quad (62)$$

$$\phi = \phi_0 \left(1 - \frac{y^2}{b^2} \right) \quad (63)$$

$$\chi = \chi_0 \left(1 - \frac{y^2}{b^2} \right) \quad (64)$$

$$\psi = \psi_0 \left(1 - \frac{y^2}{b^2} \right) \quad (65)$$

$$\omega = \omega_0 \left(1 - \frac{y^2}{b^2} \right) \quad (66)$$

$$\sigma = \sigma_0 \left(1 - \frac{y^2}{b^2} \right) \quad (67)$$

$$\tau = \tau_0 \left(1 - \frac{y^2}{b^2} \right) \quad (68)$$

$$\nu = \nu_0 \left(1 - \frac{y^2}{b^2} \right) \quad (69)$$

$$\xi = \xi_0 \left(1 - \frac{y^2}{b^2} \right) \quad (70)$$

$$\eta = \eta_0 \left(1 - \frac{y^2}{b^2} \right) \quad (71)$$

$$\theta = \theta_0 \left(1 - \frac{y^2}{b^2} \right) \quad (72)$$

$$\phi = \phi_0 \left(1 - \frac{y^2}{b^2} \right) \quad (73)$$

$$\chi = \chi_0 \left(1 - \frac{y^2}{b^2} \right) \quad (74)$$

$$\psi = \psi_0 \left(1 - \frac{y^2}{b^2} \right) \quad (75)$$

$$\omega = \omega_0 \left(1 - \frac{y^2}{b^2} \right) \quad (76)$$

$$\sigma = \sigma_0 \left(1 - \frac{y^2}{b^2} \right) \quad (77)$$

$$\tau = \tau_0 \left(1 - \frac{y^2}{b^2} \right) \quad (78)$$

$$\nu = \nu_0 \left(1 - \frac{y^2}{b^2} \right) \quad (79)$$

$$\xi = \xi_0 \left(1 - \frac{y^2}{b^2} \right) \quad (80)$$

$$\eta = \eta_0 \left(1 - \frac{y^2}{b^2} \right) \quad (81)$$

$$\theta = \theta_0 \left(1 - \frac{y^2}{b^2} \right) \quad (82)$$

$$\phi = \phi_0 \left(1 - \frac{y^2}{b^2} \right) \quad (83)$$

$$\chi = \chi_0 \left(1 - \frac{y^2}{b^2} \right) \quad (84)$$

$$\psi = \psi_0 \left(1 - \frac{y^2}{b^2} \right) \quad (85)$$

$$\omega = \omega_0 \left(1 - \frac{y^2}{b^2} \right) \quad (86)$$

$$\sigma = \sigma_0 \left(1 - \frac{y^2}{b^2} \right) \quad (87)$$

$$\tau = \tau_0 \left(1 - \frac{y^2}{b^2} \right) \quad (88)$$